J Therm Anal Calorim (2012) 109:1193–1201
DOI 10.1007/s10973-012-2283-9

# Thermal analysis of spider silk inspired di-block copolymers in the glass transition region by TMDSC

**Wenwen Huang · Sreevidhya Krishnaji · David Kaplan · Peggy Cebe**

NATAS2011 Conference Special Chapter


**Abstract** We used advanced thermal analysis methods to characterize a new family of A-B di-block copolymers based on the amino acid sequences of *Nephila clavipes* major ampulate dragline spider silk. Using temperature modulated differential scanning calorimetry with a thermal cycling method and thermogravimetry, we captured the effect of bound water acting as a plasticizer for spider silk-like biopolymer films which had been cast from water solution and then dried. A low glass transition because of bound water removal was observed in the first heating cycle, after which, a shift of glass transition was observed in A-block film due to crystallization and annealing, and in BA film due to annealing. No shift of glass transition after bound water removal was observed in B-block film. The reversing heat capacities, $C_p$, for temperatures below and above the glass transition were measured and compared to the calculated values. The solid state heat capacity was modeled below $T_g$, based on the vibrational motions of the constituent poly(amino acid)s, heat capacities of which are known from the ATHAS Data Bank. Excellent agreement was found between the measured and calculated values of the heat capacity, showing that this model can serve as a standard method to predict the solid state $C_p$ for other biologically inspired block-copolymers. We also calculated the liquid state heat capacities of the 100% amorphous biopolymer at $T_g$, and this predicted value can be use to determined the crystallinity of protein-based materials.

**Keywords** Nephila Clavipes spider dragline silk · Block copolymer · Heat capacity · Glass transition · Temperature modulated differential scanning calorimetry · X-ray diffraction

W. Huang · P. Cebe (✉)
Department of Physics and Astronomy, Center for Nanoscopic Physics, Tufts University, Medford, MA 02155, USA
e-mail: peggy.cebe@tufts.edu

S. Krishnaji
Department of Chemistry, Tufts University, Medford, MA 02155, USA

D. Kaplan
Department of Biomedical Engineering, Tufts University, Medford, MA 02155, USA

## Introduction

The dragline of *Nephila Clavipes* has been widely studied because of its potential application in tissue engineering and drug delivery [1–3]. Recent studies suggest that at least two proteins, the major ampullate spidroins 1 (MaSp1), and major ampullate spidroins 2 (MaSp2), comprise the spider dragline silk fiber [4]. MaSp1 and MaSp2 proteins are modular in nature. Both of them consist of three specific structural motifs with highly repetitive consensus sequences [4]: (1) the poly-alanine GA/$A_n$ motif, (2) the GG*X* motif in MaSp1 or GPGG*X* motif in MaSp2, and (3) the N-terminus and C-terminus. Hayashi and co-workers extensively studied the correlation between the sequence, structure, and the mechanical properties of spider silk proteins [5, 6]. They associated these motifs with its impact on the mechanical properties of a silk fiber. In particular, alanine-rich "crystalline module," gives the fiber tensile strength and toughness, and the GG*X* and GPGG*X* "elasticity module," stabilized the fiber and provided the elasticity and extensibility. To draw a correlation between the sequence, structure, and thermodynamic properties of biomacromolecules, the phase transitions of silk worm silk fibroin have been well

studied using quantitative thermal analysis [7–9]. Pyda et al. [10–12] also interpreted the thermodynamic properties of biomacromolecules by the underlying molecular motion.

Inspired by these ideas, we studied the phase transition of alanine-rich A-block which is similar to the "crystalline module," glycine rich B-block which is similar to the "elastic module" and their block copolymer BA using temperature-modulated differential scanning calorimetry (TMDSC). In the present study, we investigate the thermodynamic properties in the range of the glass transition temperature, $T_g$. As reported, bound water plasticizes the silk fibroin films inducing a low $T_g$ during heating, and the water content within the silk film affects the value of this water-induced $T_g$ [8, 11, 13]. To avoid this effect, we used a vacuum oven and a thermal cycling method [13, 14] to remove both the surface and the bound water. This cycling process was monitored by TMDSC and both plasticization effect of bound water and the shift of $T_g$ due to crystallization and annealing, were captured. The water content lost during heating was also assessed by thermogravimetry (TG).

In this study, we also investigated the thermodynamic properties of A-block, B-block, and BA block copolymer based on the amino acid molecular motion. The baseline of the heat capacity, and the solid and liquid $C_p$ values of biomacromolecules can be predicted using the advanced thermal analysis system (ATHAS) data bank and the amino acid structures as described previously [11, 15, 16]. In brief, below $T_g$, the solid $C_p$ is based only on the atomic vibrational motion; while above $T_g$, the liquid $C_p$ is based on both the vibrational motion and the large-amplitude conformational motion [15]. Following this method, we calculated the solid and liquid $C_p$ values of A-block, B-block, and BA block copolymer. Excellent agreement was found between the calculated and the measured values of the heat capacity by TMDSC. During heating, the glass transition is observed as an endothermic step in the heat flow, corresponding to an increase in the heat capacity. The magnitude of the step change at $T_g$ is proportional to the amount of material changing from the solid to the liquid state [17, 18]. Using the measured $C_p$ values from TMDSC and the calculated change of heat capacity step at $T_g$ of 100% amorphous sample based on the amino acid molecular motion, we also determined the crystallinity of the spider silk-like biomaterial. The result was confirmed by wide angle X-ray diffraction (WAXD). From this fundamental study of the correlation between thermal properties and amino acid motifs, we anticipate that these results will provide an insight for the design and control of the smart materials having similar properties as spider silks using well-controlled protein sequences.

## Experimental section

### Materials and preparation

A-block, B-block, and spider silk-like block copolymers BA without histidine tags were synthesized by the Tufts University Protein Core Facility (TUCF) on an Applied Biosystems ABI 431 peptide synthesizer employing traditional F-moc chemistry and purified. In order to prevent cyclization of the peptides, the C-terminus was modified to an amide. Synthetic peptides were purified by HPLC (2.1 mm $C_{18}$ column). The synthetic peptides were run on SDS-PAGE and stained with Colloidal Blue and silver stain to confirm their purity. MALDI-TOF was used to confirm protein identity. The materials were obtained in solid form after lyophilizing and then cast into films from water solution for the purpose of our studies. The number of residues, the amino acid sequences, and the calculated and measured molecular weight by MALDI-TOF of A-block, B-block, and BA, are listed in Table 1.

### Differential scanning calorimetry

TMDSC measurements were carried out using a TA Instruments Q100 DSC equipped with a refrigerated cooling system to obtain the total and reversing heat flow. Indium was employed for calibrating the heat flow and temperature before sample measurements. In the thermal cycling and heat capacity studies, the experiments were performed at a heating rate 2 °C $min^{-1}$ with a modulation period of 60 s, and a temperature amplitude of 0.318 °C. A nitrogen purge gas was used at a flow rate of 50 mL $min^{-1}$. The sample mass weighed about 2–3 mg. Endotherms were presented with downward deflection in heat flow versus temperature scans.

For the quantitative DSC studies of the heat capacity, a three-run method [15, 19] was carried out: (1) the first run

**Table 1** Amino acid sequence and molecular weight of A-block, B-block and BA

| Code | # Residues | Sequence | $M_w$/Da | $M_w$ (MALDI)/Da |
|---|---|---|---|---|
| A | 17 | MASGAGAAAAAGGAGTS | 1278.3 | 1279.73 |
| B | 25 | MAS**QGGYGGLGSQGSGRGGLGGQTS** | 2227.4 | 2228.46 |
| BA | 39 | MAS**QGGYGGLGSQGSGRGGLGGQTS**GAGAAAAAGGAGTS | 3198.3 | 3199.73 |

*Note* Underlined sequences indicate the A-block (without modified C-terminus), and bold sequences indicate the B-block (without modified C-terminus)

was with the empty Al reference pan and the empty Al sample pan, for correcting the asymmetry and baseline of the DSC; (2) the second run was with the empty Al reference pan and Al pan filled with sapphire standard for calibration; and (3) the third run was with the empty Al reference pan, and the Al pan filled with sample. After a steady state was obtained, the heat capacity of the sample can be determined by

$$\left|mC_{\mathrm{p}} + C_{\mathrm{s}} - C_{\mathrm{r}} \pm \Delta C_{\mathrm{cell}}\right| = \frac{A_{\mathrm{AF}}}{A} K'' \tag{1}$$

where $C_{\mathrm{s}}$ and $C_{\mathrm{r}}$ are the heat capacities of the sample pan and empty reference pan, respectively, and $\Delta C_{\mathrm{cell}}$ is the cell asymmetry correction which can be obtained in the first run; $K''$ is the calibration constant related to the experimental conditions determined by the sapphire standard in the second run; $mC_{\mathrm{p}}$ is the heat capacity of the sample of mass, $m$, and the specific heat capacity, $C_{\mathrm{p}}$, which is calculated from the third run. $A_{\mathrm{HF}}$ is the heat flow amplitude, and $A$ is the sample temperature modulation amplitude.

### TG

TG was performed on a TA Instruments Q500 thermogravimetric analyzer at a heating rate of 2 °C $\mathrm{min}^{-1}$ from room temperature to 300 °C in a nitrogen purge gas flow of 50.0 mL $\mathrm{min}^{-1}$. To prevent the powdered sample from being blown out of the pan by nitrogen gas flow, the samples were encapsulated in aluminum DSC pans during heating. Several holes were made on DSC lids to let the sample surface be exposed to the atmosphere, to allow the degradation products escape. Before each run, the empty pan with platinum TGA basket was used to calibrate the zero point of the total mass. The initial sample mass ranged between 4.0 and 5.0 mg.

### WAXD

WAXD was performed on a Bruker GADDS D8 Discover X-ray diffractometer (wavelength $\lambda = 0.154$ nm) operated at 40 kV and 20 mA. Scattering angle, $2\theta$, was calibrated by silicon (111) peak at 28.444°. The scan time used was 1,800 s per sample. The scattering angle, $2\theta$, ranged from 5 to 29°. The air background was subtracted from the original scan for each sample. To calculate the crystallinity index, $\phi_{\mathrm{ci}}$, the two-dimensional WAXD patterns were converted into one-dimensional scans by integrating over the azimuthal angle. Then, the Lorentz-corrected WAXD peak intensity, $I(q)q^2$, was fitted by Gaussian wave functions as described previously [20, 21]. The crystallinity index, $\phi_{ci}$, was calculated using the area of the crystal peaks, $A_{\mathrm{crystal}}$, divided by the total area, $A_{\mathrm{total}}$:

$$\phi_{\mathrm{ci}} = \frac{A_{\mathrm{crystal}}}{A_{\mathrm{crystal}} + A_{\mathrm{amorphous}}} = \frac{A_{\mathrm{crystal}}}{A_{\mathrm{total}}} \tag{2}$$

## Results and discussion

### Thermal cycling for surface water and bound water removal

The state of water absorbed in polymeric systems has been extensively studied [13, 22, 23] using various techniques [7, 13]. It has been reported that water in polymeric systems can be classified into three types [13, 23]: (i) free water, (ii) freezable loosely bound water, and (iii) non-freezing bound water. To determine the water content in A-block, B-block, and BA, TG measurements were performed. The water-cast films of A-block, B-block, and BA were stored in desiccators before the experiments. A portion of these films were enclosed in aluminum DSC pans and heated at 2 °C $\mathrm{min}^{-1}$ in TG; the rest of these films were enclosed in the aluminum DSC pans, annealed in vacuum oven at 30 °C overnight, and then heated in TG at the same heating rate of 2 °C $\mathrm{min}^{-1}$. The empty pan with platinum TGA basket was used to reset the zero point of the total mass. Figure 1a, b, c, shows the TG curves of A-block, B-block, and BA, respectively, before (dashed curves) and after (solid curves) annealing in vacuum oven.

As observed from Fig. 1, the un-annealed samples lose mass faster than the annealed samples, which suggest that the surface water in A-block, B-block, and BA film was removed by annealing samples in the vacuum oven. By subtracting the mass of the remaining fraction of the un-annealed from that of the annealed films, we can estimate that, for the un-annealed samples in hydrophobic A-block film, the free water accounts for about 4.9% of the total mass; in hydrophilic B-block film, the free water is about 5.4% of the total mass; and in block copolymer BA, the free water takes about 3.0% of the film total mass (as shown in the inset plots of Fig. 1). Results indicate that in A-block, B-block, and BA films, surface water is not intimately bound to the polymer chain and can be easily removed by storing the samples in the vacuum oven.

After annealing in the vacuum oven, mass loss still was observed in the A-block, B-block, and BA films during heating because of the bound water removal (as shown in Fig. 1 solid curves). By heating at 2 °C $\mathrm{min}^{-1}$, the annealed films start releasing water molecules into the environment at about 40 °C. As the temperature increases, more and more water escapes, and the total mass of the films decreases. Until about 100 °C, a total mass loss of $\sim$1% bound water was lost from the A-block film. Owing to the hydrophilic nature of the B-block film, the bonding interaction between water molecules and the polymer

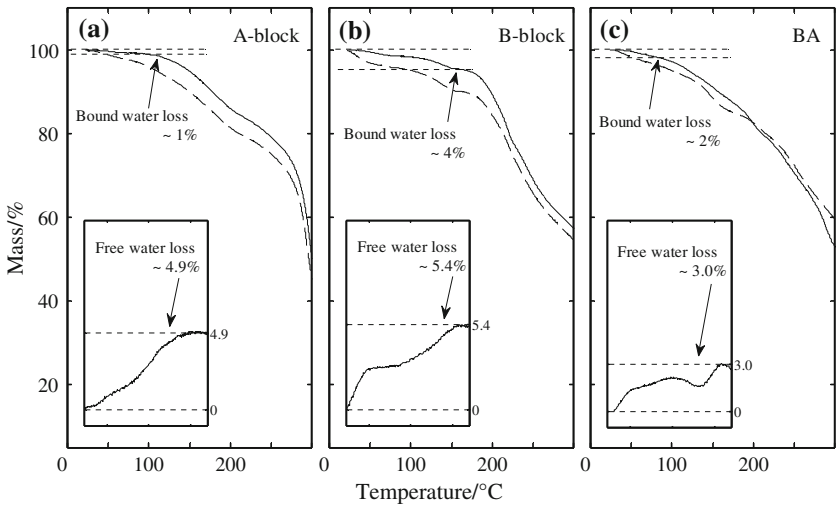


**Fig. 1** Thermogravimetric curves of mass remaining versus temperature at 2 °C $min^{-1}$ for: **a** A-block, **b** B-block, and **c** BA before (*dashed curve*) and after (*solid curve*) annealing in a vacuum oven at 30 °C. The *inset* plots of mass remaining versus temperature depict the differences between the remaining masses of the annealed (*solid curve*) and un-annealed samples (*dashed curve*)

chains is stronger than that in the A-block film. B-block film will release water molecules at a higher temperature range, from about 40 to 150 °C, and with a larger amount of the total mass loss of 4% bound water. BA lost about a total mass loss of 2% bound water during heating. This can be compared with the reconstituted silk fibroin protein, which contains around 5% of bound water independent of the heating rate [13].

From the previous DSC studies [7, 8, 11, 13], bound water inside the silk films will induce a low $T_g$ during heating, and the water content in the silk film will affect the temperature value of this water-induced glass transition. To study the effect of bound water on the spider silk-like biopolymers, the surface water absorbed in our samples was removed by annealing the samples in vacuum oven at 30 °C overnight before DSC measurements. Then, we used seven continuous heating cycles to monitor the change of the total and reversing heat flows during water removal by TMDSC. All the seven heating cycles started from the same temperature, $T_{start} = -50$ °C, and the cycles 1–7 ended at steadily increasing ending temperatures of $T_{end} = 100$, 120, 140, 150, 160, 170, and 230, respectively. Figure 2a, b, c shows the total heat flows of A-block, B-block, and BA, respectively, during thermal cycling. Because the total heat flow curves of the cycles 2–7 overlap each other in the temperature ranging from −50 to 0 °C, the total heat flows for the cycles 2–7 were shifted upward for clarity.

The bound water removal process analyzed using the total heat flow is shown in Fig. 2. As the temperature increases slowly, the bound water molecules evaporated, which results in not only an absorption of enthalpy but also a mass decrease. To obtain an accurate sample mass, the sample mass of each run was corrected according to the TG profiles with the same heating rate of 2 °C $min^{-1}$. In the first heating process, no melting peak around 0 °C was observed. This indicates that after keeping the films in vacuum oven overnight, the free water was completely removed [7]. During this process, a very broad endothermic peak in the temperature range of 0–100 °C was observed. This can be attributed to the interaction between intermolecular weakly bound water molecules and the polymer chains [24, 25]. In the second heating process, the total heat flow curve is almost a straight line. This indicates that the non-freezing bounded water residue is also removed. Distinct $T_g$ values for A-block, B-block, and BA in the absence of the effect of water were obtained in the cycles 3–7.

Figure 3a, b, c shows the TMDSC reversing heat flows of A-block, B-block and BA, respectively, during the thermal cycling study. The reversing heat flows in the cycles 2–7 were shifted upward for clarity. By the analysis of the reversing heat flows, we can avoid the non-reversing endothermic effect from water evaporation, and only focus on the glass transition behavior in the thermal cycling process.

In Fig. 3a, the $T_g$ of A-block shifted from 130 to 156 °C, and the reversing heat flow step size at $T_g$ became smaller for the cycles 4–7. Results indicate that A-block film was enabled to crystallize during the slow heating process. Owing to the restriction induced by $\beta$ sheet formation on the mobility of the remaining less-ordered segments and the free volume reduction from thermal annealing, $T_g$ in A-block shifts to a higher temperature [26, 27]. As shown in Fig. 3a, the $\beta$ sheet in the crystalline regions also acted as physical cross-linker causing a broadening of the relaxation process at $T_g$. This result is consistent with what had been observed in the reconstituted silk fibroin protein films [19, 28]. In Fig. 3b, the $T_g$ of B-block is very stable at 138 °C from the cycles 3–7, and the step sizes of change of the reversing heat flows at $T_g$ are the same. Because B-block film sample is almost fully amorphous before DSC measurement (determined from WAXD) and no $\beta$ sheet crystals were formed in the thermal cycling process, the

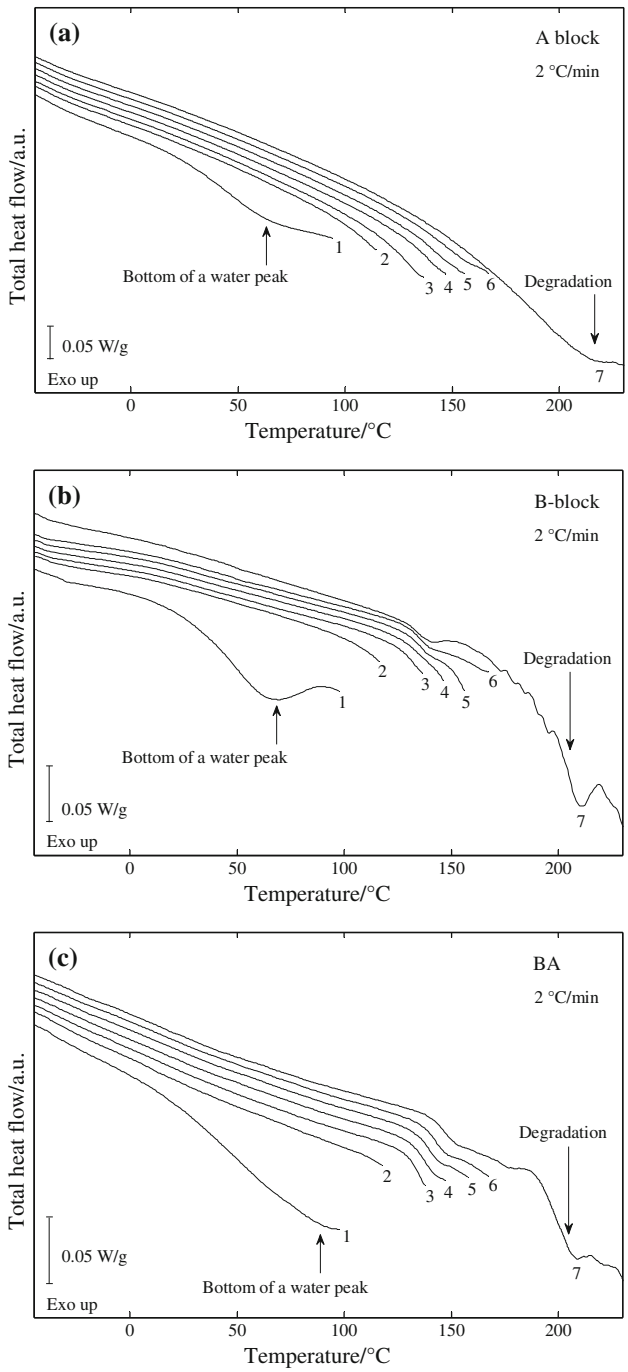


**Fig. 2** TMDSC total heat flow at 2 °C $min^{-1}$ versus temperature during seven thermal cycles, for: **a** A-block, **b** B-block, and **c** BA. Endotherms are presented with downward deflection

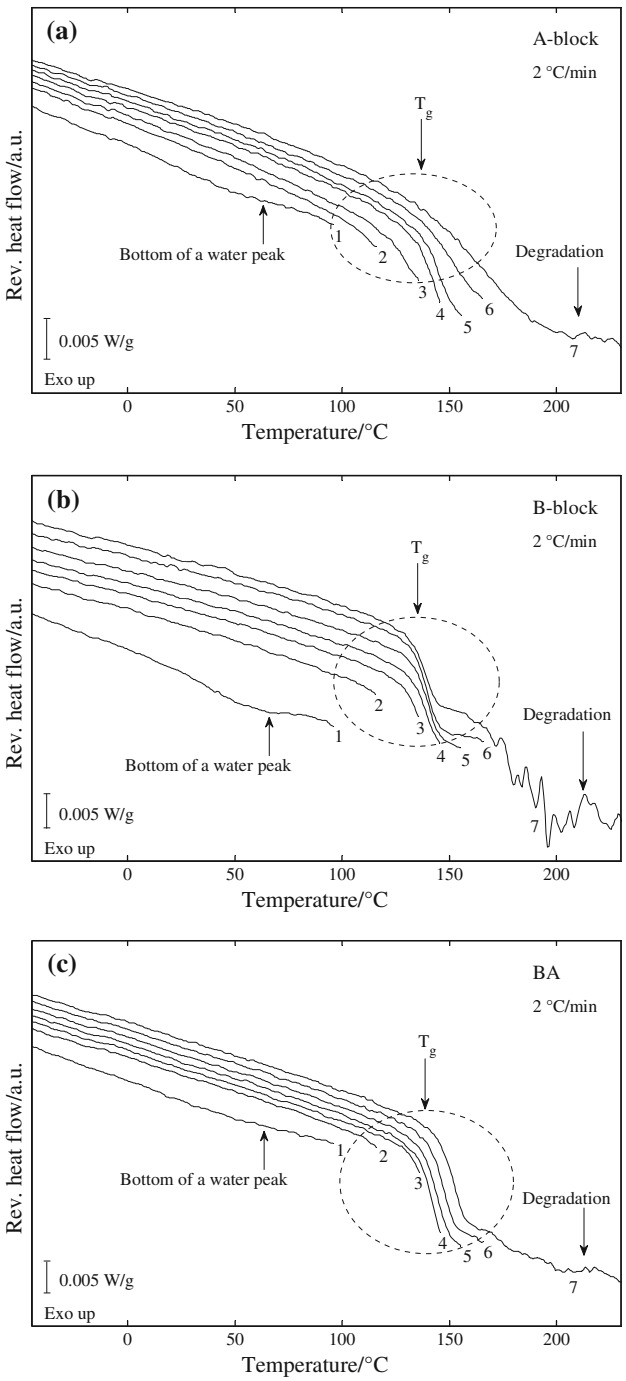


**Fig. 3** TMDSC reversing heat flow versus temperature at 2 °C $min^{-1}$ during seven thermal cycles, for: **a** A-block, **b** B-block, and **c** BA. Endotherms are presented with downward deflection

restrictions on the chain mobility are almost unchanged. Thus, the value of $T_g$ of B-block remains constant. In Fig. 3c, the $T_g$ of BA block copolymer is also shifted from 137 to 154 °C in the cycles 3–7, and the step sizes of reversing heat flow change at $T_g$ are the same. In BA, the films did not crystallize during the heating cycles. However, because the block copolymer BA has two subunits linked by covalent bonds, the backbone of its polymer chain exhibits higher flexibility than that of B-block. Annealing of BA film reduced the free volume in between the polymer chains and thus confined the mobility of the remaining less-ordered segments, which leads to a higher $T_g$ [26, 27]. From Figs. 2 and 3, we can conclude that (1) bound water cannot be completely removed by annealing

in the vacuum oven, and a low glass transition in the temperature range from 50 to 80 °C is formed because of the intermolecular weakly bound water; (2) the shift of the glass transition temperature during slow heating after bound water removal can be observed in A-block film because of both crystallization and annealing, as well as in BA film because of annealing; and, (3) no shift of glass transition during slow heating after bound water removal can be observed in B-block film.

## Heat capacity of spider silk-like motifs and their block copolymer

The calculation of the heat capacities of polypeptide and silk proteins has been discussed in detail previously [11, 15]. In brief, the solid $C_p$ from 0 K to the onset of glass transition is based on the assumption that only the vibrational motion from the constituent amino acid residues contributes to the heat capacity. The solid $C_p$ value can be estimated as the sum of products of the vibrational heat capacities of the individual amino acid residues, $C_p(i)$, times the total number of each type of amino acid residues found in the sequence, $N_i$:

$$C_p(\text{solid}) = C_p(\text{vibrational}) = \sum_i N_i C_p(i) \tag{3}$$

The solid $C_p$ for individual amino acid monomer, $C_p(i)$, can be found directly or predicted from the data in ATHAS data bank [15, 16, 29].

From the amino acid sequences of A-block and B-block in Table 1, the solid $C_p$ can be calculated as

$$C_p^{\text{A-block}}(\text{solid}) = 8 \times C_p(\text{Ala}) + 5 \times C_p(\text{Gly}) + 2 \times C_p(\text{Ser}) + C_p(\text{Met}) + C_p(\text{Thr}) \tag{4}$$

$$C_p^{\text{B-block}}(\text{solid}) = 11 \times C_p(\text{Gly}) + 4 \times C_p(\text{Ser}) + 3 \times C_p(\text{Gln}) + 2 \times C_p(\text{Leu}) + C_p(\text{Ala}) + C_p(\text{Arg}) + C_p(\text{Met}) + C_p(\text{Thr}) + C_p(\text{Tyr}) \tag{5}$$

The solid $C_p$ of BA block copolymer is just the sum of the solid $C_p$ values of the A-block and B-block after subtracting the solid $C_p$ of the one C-terminus:

$$C_p^{\text{BA}}(\text{solid}) = C_p^{\text{A-block}}(\text{solid}) + C_p^{\text{B-block}}(\text{solid}) - (C_p(\text{Met}) + C_p(\text{Ala}) + C_p(\text{Ser})) \tag{6}$$

The solid $C_p$ [J (mol K)$^{-1}$] is the molar heat capacity as mentioned in Eqs. 3–6, and can be converted to the specific heat capacity, $c_p$ [J (g °C)$^{-1}$], by dividing it by the molecular weight, $M_w$:

$$c_p(\text{solid}) = C_p(\text{solid})/M_w \tag{7}$$

The liquid $C_p$ at $T_g$ of 100% amorphous sample can be estimated by their the amino acid sequence and chemical structure. Each mobile unit (i.e., each rotational bond) in the polymer chain on average contributes 11 J (mol K)$^{-1}$ [18] to the change of heat capacity, $\Delta C_{p0}$, at $T_g$, and these

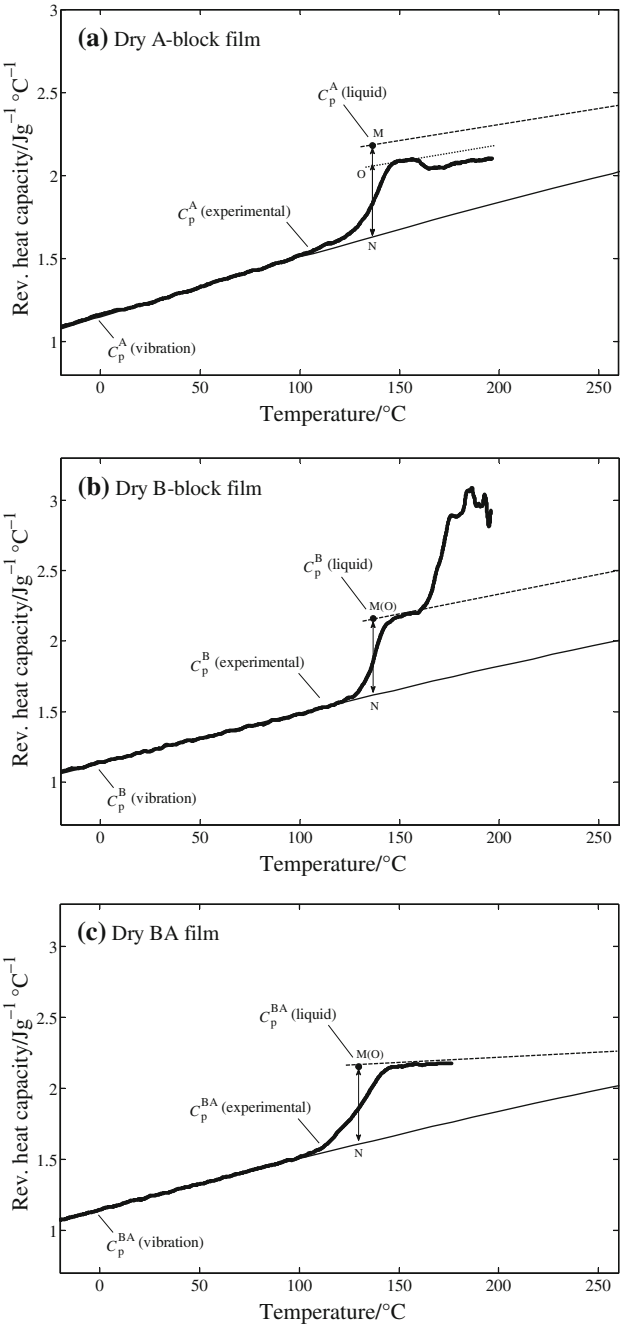


**Fig. 4** The measured and calculated apparent reversing heat capacity versus temperature, after annealing at 120 °C, for dry films of: **a** A-block, **b** B-block, and **c** BA. *Heavy curve* $C_p$(experimental), *thin solid curve* $C_p$(vibrational), *filled circles* $C_p$(liquid) calculated at $T_g$ taken at half height of the heat capacity step. *Dashed lines* are the extrapolated best *fit lines* to experimental curve above $T_g$. *Line ON* is the measured heat capacity step, $\Delta C_p$, at $T_g$ from TMDSC, and *line MN* is the calculated heat capacity step $\Delta C_{p0}$, at $T_g$ based on the number of mobile units for 100% amorphous sample

rotational degrees of freedom contribute about 91% to the $\Delta C_p$ [15]. Thus, the $\Delta C_{p0}$ at $T_g$ can be calculated. The slope of the liquid $C_p$ is obtained from the tangent of the $C_p$ (experiment) above $T_g$.

Next, to eliminate the bound water, the samples were annealed at 120 °C for 60 min. In Fig. 4a, b, c, the measured heat capacities (shown in heavy solid curve) agree very well with the calculated solid $c_p$ (thin solid lines) and calculated liquid $c_p$ at $T_g$ (filled circle). This agreement supports the conclusion that only the vibrational motion of the amino acid residues contributes to the solid $C_p$ below $T_g$, and the rotational and translational motions must be taken into consideration when estimating the liquid $C_p$.

The degree of crystallinity is also determined from the TMDSC measurements and the heat capacity model, and the results are summarized in Table 2. During heating, the step change of $C_p$ at $T_g$ only comes from the non-crystalline region of the sample [30]. On the assumption of a two-phase model comprising crystals and mobile non-crystalline chains, the degree of crystallinity, $\varphi_c$, can be calculated from

$$\varphi_C = 1 - \varphi_M = 1 - (\Delta C_p/\Delta C_{p0})|_{T_g} \quad (8)$$

where $\Delta C_p$ is the heat capacity step measured at $T_g$ from TMDSC (shown as line *ON* in Fig. 4 and line *ON* overlap line *MN* in Fig. 4b, c), and $\Delta C_{p0}$ is the calculated heat capacity step at $T_g$ based on the number of mobile units for 100% amorphous sample (shown as line *MN* in Fig. 4).

To verify the heat capacity model, WAXD was also employed to determine the crystallinity index of A-block, B-block, and BA. The inset plots of Fig. 5a, b, c show the 2-D WAXD pattern of A-block, B-block, and BA, respectively. The 2-D WAXD patterns were then radially integrated into 1-D WAXD intensity. In Fig. 5a, three major crystalline peaks were observed for A-block film at $q = 12.09$, 14.51, and 17.06 $nm^{-1}$ corresponding to lattice distances of $\beta$ sheet $d_{200} = 0.520$ nm, $d_{120} = 0.433$ nm, and $d_{121} = 0.371$ nm, respectively [31]. A broad peak of the amorphous halo centered at $q = 15.57$ $nm^{-1}$ was also observed for all the samples as shown in Fig. 5a–c(c). By fitting the Lorentz-corrected WAXD peak intensity $I(q)q^2$ vs.q (open circles in Fig. 5) with Gaussian wave functions (solid and dashed curves in Fig. 5) as described previously [20], the crystallinity index, $_{ci}$, was calculated using the area of the crystal peaks to the total area by Eq. 2, and the result is summarized in Table 2. For the A-block, the

**Table 2** Crystallinity determined by TMDSC and WAXD of A-block, B-block and BA

| Sample | $\Delta C_p^{Measured}$/ $Jg^{-1}{}^{\circ}C^{-1}$ (± 0.001) | $\Delta C_p^{Calculated}$/ $Jg^{-1}{}^{\circ}C^{-1}$ (± 0.001) | $\varphi_{ci}$ (DSC) (± 0.02) | $\phi_c$ (WAXD) (± 0.03) |
|---|---|---|---|---|
| A | 0.397 | 0.539 | 0.27 | 0.31 |
| B | 0.539 | 0.543 | 0.01 | 0.03 |
| BA | 0.545 | 0.544 | 0 | 0.01 |

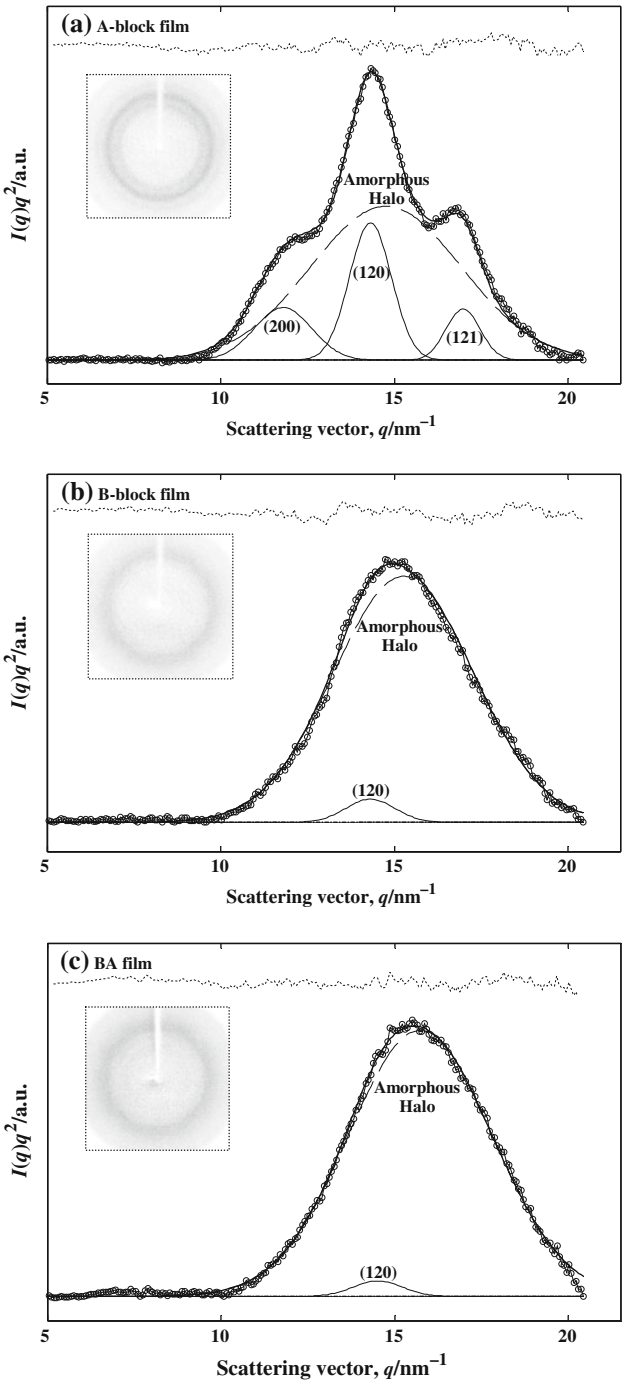


**Fig. 5** Deconvolution of the Lorentz-corrected WAXD intensity, $I(q)q2$ versus $q$, using Gaussian wave functions for **a** A-block, **b** B-block, and **c** BA (*Open circles* measured data, *heavy curves* summation of Gaussian peaks, *thin solid curves* individual crystalline Gaussian peaks, *dashed curves* amorphous Gaussian peaks, *dotted lines at the top* the residual between the fitted curve and measured curve). The *inserts* shows the 2-D WAXD patterns

degree of crystallinity is about 30%, and for the B-block and their block copolymer BA, the crystallinity is almost zero. The amorphous B-block hinders the chain folding of A-block in BA block copolymer and BA remains amorphous before and after the thermal cycling process.

## Conclusions

The thermal properties of spider silk-like motifs A-block and B-block, and their block copolymer BA were studied using TMDSC. Water content in spider silk-like biopolymer was analyzed by TG. Results indicate that by annealing samples in the vacuum oven at 30 °C, the surface water can be removed, but the bound water will remain in the sample films. The bound water removal process was studied using a thermal cycling method. A low glass transition in the temperature range from 50 to 80 °C was observed in the first cycle because of bound water removal, after which, a shift of glass transition can be observed in the A-block film because of crystallization and annealing, and in the BA film because of thermal annealing. No shift of glass transition during slow heating after bound water removal was observed in B-block film.

In this study, we also studied the thermodynamic properties of A-block, B-block and BA block copolymer based on the amino acid molecular motion. The solid $C_p$ and liquid $C_p$ were predicted by using the ATHAS data bank and the amino acid structures. Excellent agreement was found between the calculated and measured values of the heat capacity. We also used the heat capacity model to calculate the degree of crystallinity from TMDSC, and the result was confirmed by WAXD. For the "crystalline module" like A-block, the degree of crystallinity is about 30%, and for the "elastic module" like B-block and their block copolymer BA, the crystallinity is almost zero. The amorphous B-block hinders the chain folding of the A-block in the BA block copolymer, and the BA remains amorphous before and after the thermal cycling process.

**Acknowledgements** The authors acknowledge the support provided from the National Science Foundation, Division of Chemical, Bioengineering, Environmental, and Transport Systems, through CBET-0828028. The thermal analysis instrumentation study was supported by the MRI Program under DMR-0520655.

## References

1. Altman GH, Diaz F, Jakuba C, Calabro T, Horan RL, Chen JS, Lu H, Richmond J, Kaplan DL. Silk-based biomaterials. Biomaterials. 2003;24(3):401–16.
2. Kluge JA, Rabotyagova U, Leisk GG, Kaplan DL. Spider silks and their applications. Trends Biotechnol. 2008;26(5):244–51.
3. Krishnaji ST, Huang WW, Rabotyagova O, Kharlampieva E, Choi I, Tsukruk VV, Naik R, Cebe P, Kaplan DL. Thin film assembly of spider silk-like block copolymers. Langmuir. 2011;27(3):1000–8.
4. McGrath K, Kaplan D. Protein-based materials. Boston: Birkhäuser; 1997.
5. Hayashi CY, Shipley NH, Lewis RV. Hypotheses that correlate the sequence, structure, and mechanical properties of spider silk proteins. Int J Biol Macromol. 1999;24(2–3):271–5.
6. Hayashi CY, Lewis RV. Molecular architecture and evolution of a modular spider silk protein gene. Science. 2000;287(5457):1477–9.
7. Lee KY, Ha WS. DSC studies on bound water in silk fibroin/S-carboxymethyl kerateine blend films. Polymer. 1999;40(14):4131–4.
8. Hu X, Kaplan D, Cebe P. Dynamic protein-water relationships during beta-sheet formation. Macromolecules. 2008;41(11):3939–48.
9. Hu X, Lu Q, Kaplan DL, Cebe P. Microphase separation controlled beta-sheet crystallization kinetics in fibrous proteins. Macromolecules. 2009;42(6):2079–87.
10. Pyda M. Conformational contribution to the heat capacity of the starch and water system. J Polym Sci Part B. 2001;39(23):3038–54.
11. Pyda M, Hu X, Cebe P. Heat capacity of silk fibroin based on the vibrational motion of poly(amino acid)s in the presence and absence of water. Macromolecules. 2008;41(13):4786–93.
12. Pyda M. Conformational heat capacity of interacting systems of polymer and water. Macromolecules. 2002;35(10):4009–16.
13. Hu X, Kaplan D, Cebe P. Effect of water on the thermal properties of silk fibroin. Thermochim Acta. 2007;461(1–2):137–44.
14. Hu X, Kaplan D, Cebe P. Thermal analysis of protein-metallic ion systems. J Therm Anal Calorim. 2009;96(3):827–34.
15. Huang WW, Krishnaji S, Hu X, Kaplan D, Cebe P. Heat capacity of spider silk-like block copolymers. Macromolecules. 2011;44(13):5299–309.
16. Pyda M The advanced thermal analysis system (ATHAS) data bank. http://athas.prz.rzeszow.pl/Default.aspx?op=db. Accessed 02 2011.
17. Wunderlich B. Study of the change in specific heat of monomeric and polymeric glasses during the glass. J Phys Chem. 1960;64(8):1052–6.
18. Wunderlich B. Thermal analysis of polymeric materials. Berlin: Springer; 2005.
19. Hu X, Kaplan D, Cebe P. Determining beta-sheet crystallinity in fibrous proteins by thermal analysis and infrared spectroscopy. Macromolecules. 2006;39(18):6161–70.
20. Huang WW, Edenzon K, Fernandez L, Razmpour S, Woodburn J, Cebe P. Nanocomposites of poly(vinylidene fluoride) with multiwalled carbon nanotubes. J Appl Polym Sci. 2010;115(6):3238–48.
21. Buckley J, Cebe P, Cherdack D, Crawford J, Ince BS, Jenkins M, Pan JJ, Reveley M, Washington N, Wolchover N. Nanocomposites of poly(vinylidene fluoride) with organically modified silicate. Polymer. 2006;47(7):2411–22.
22. Hodge RM, Bastow TJ, Edward GH, Simon GP, Hill AJ. Free volume and the mechanism of plasticization in water-swollen poly(vinyl alcohol). Macromolecules. 1996;29(25):8137–43.
23. Kim YS, Dong LM, Hickner MA, Glass TE, Webb V, McGrath JE. State of water in disulfonated poly(arylene ether sulfone) copolymers and a perfluorosulfonic acid copolymer (nafion) and its effect on physical and electrochemical properties. Macromolecules. 2003;36(17):6281–5.
24. Motta A, Fambri L, Migliaresi C. Regenerated silk fibroin films: thermal and dynamic mechanical analysis. Macromol Chem Phys. 2002;203(10–11):1658–65.
25. Randzio SL, Flis-Kabulska I, Grolier JPE. Reexamination of phase transformations in the starch-water system. Macromolecules. 2002;35(23):8852–9.

26. Lu SX, Cebe P. Effects of annealing on the disappearance and creation of constrained amorphous phase. Polymer. 1996;37(21): 4857–63.
27. Pyda M, Wunderlich B. Reversing and nonreversing heat capacity of poly(lactic acid) in the glass transition region by TMDSC. Macromolecules. 2005;38(25):10472–9.
28. Chen H, Hu X, Cebe P. Thermal properties and phase transitions in blends of nylon-6 with silk fibroin. J Therm Anal Calorim. 2008;93(1):201–6.
29. Wunderlich B. The ATHAS database on heat-capacities of polymers. Pure Appl Chem. 1995;67(6):1019–26.
30. Menczel J, Wunderlich B. Heat-capacity hysteresis of semi-crystalline macromolecular glasses. J Polym Sci Part C. 1981;19(5):261–4.
31. Warwicker JO. Comparative studies of fibroins. 2. Crystal structures of various fibroins. J Mol Biol. 1960;2(6):350–62.